Chapter 4
Accelerated Mechanical Behavior Characterization of Structural Materials

J. Rathore, A. Imeri, E. Al Amiri, V. Shah, C. O'Brien, B. Wisner, and A. Kontsos

Abstract Qualification processes for the mechanical behavior of advanced materials depend heavily on extensive experimental testing needed to also obtain inputs to both physics-based and machine learning models. The use of full-field methods has some inherent advantages towards the direction of accelerating such qualification compared with traditional mechanical testing approaches. To demonstrate an application of this potential, a novel specimen design is produced to obtain all input parameters to a J_3-type plasticity model that can characterize the plastic behavior of any type of alloy (in terms of crystallography), while also including the effects of anisotropy and strength differential dependencies. This work presents details on how Digital Image Correlation (DIC) could be used first to obtain mechanical behavior information from tests using standardized geometries which are then used to uniquely define input parameters for the plasticity model. This information is then leveraged to accelerate the plasticity model calibration process by using Finite Element Analysis (FEA) to design a novel test specimen geometry which can produce the same information by a 4-fold reduction of the associated number of experiments. Finally, this presentation concludes with the validation of the results obtained by the use of this novel specimen and by furthermore demonstrating how the FEA model could be used to augment the DIC information by computing the components of the strain tensor that are not measured by DIC while also providing the stress tensor components and related reaction forces.

Keywords Mechanical Testing · Digital Image Correlation · Plasticity

Introduction

Novel developments and performance improvement of advanced materials are hindered by the time involved between discovery and adoption. This is particularly true for the case of advanced manufacturing materials where small changes in the feedstock, process and post-process create unpredictable changes in the resulting mechanical behavior [1, 2]. Thorough understanding of material behavior requires exhaustive testing under various loading and environment conditions[3]. Additionally, testing is also used to develop and calibrate mathematical models (e.g. constitutive laws) to be used, for example, in Finite Element Analysis (FEA). Advanced materials used in engineering applications typically experience complex stress states which cannot be captured by simple specimen geometries, as defined e.g. by common standards[4]. In addition, most conventional and standardized testing methods use point-wise global measurements such as extensometers and strain gauges to provide bulk or global information (typically stress-strain curves). Furthermore, depending on the manufacturing methods used, materials can exhibit anisotropic, differential hardening, damage and other stress-state dependent effects (e.g. triaxiality), which cause non-homogenous stress and strain fields and add difficulty in developing reliable and accurate computational models.

J. Rathore · A. Imeri · E. Al Amiri · V. Shah · A. Kontsos(✉)
Digital Engineering Hub, Department of Mechanical Engineering, Henry M. Rowan College of Engineering, Rowan University, Glassboro, NJ 08028
email: rathor12@students.rowan.edu; imeri@rowan.edu; alamir78@rowan.edu; shahva28@rowan.edu; kontsos@rowan.edu

B. Wisner · C. O'Brien
Center for Advanced Materials Processing, Department of Mechanical Engineering Russ College of Engineering and Technology, Ohio University, Athens, OH 45701
email: bwisner@ohio.edu

Emily Retzlaff et al. (eds.), *Mechanics of Additive & Advanced Manufacturing, Inverse Methods and Machine Learning, Vol. 5*,
Conference Proceedings of the Society for Experimental Mechanics Series, https://doi.org/10.13052/97887-438-0831-2_4

The emergence of non-contact optical methods such as Digital Image Correlation (DIC) has made it possible to perform full-field deformation measurements [5]. Since the 1980's DIC has been used extensively for evaluating mechanical properties of various materials at room temperatures and extreme conditions. The ability to analyze full-field measurements has the advantage of inspecting multi-stress modes present in a specimen or a part by probing specific regions of interest on the same field of view [6]. This capability has also allowed recently the design of unconventional specimen geometries that can imitate the complex loading modes found at the component level [6, 7]. This new approach of determining mechanical constitutive parameters has been coined as 'Material Testing 2.0' (MT2.0) by Pierron and Grediac [8]. Following this approach, several examples of novel specimens that capture more than one stress mode have been developed. For example, Khameneh et al. designed a specimen from which they examined the influence of tension regions and the geometry of shear region on the development of shear stress state in conjunction with FEA for fracture characterization of DP1180 steel [7]. Bensing et al. developed a specimen for evaluation of tensile and compression properties of thermoplastic polymers [6]. To further support the development of accelerated measurement of constitutive parameters, Jones et al. provided full-field DIC, and infrared thermography (IR) data tested at different rates and direction for seven unique geometries[9]. Multimodal stress state data becomes important in calibrating FEA models. For example, a general yield function developed by Lou et al. involves four stress modes analysis for computing hardening behavior that can exhibit differential and anisotropic hardening [10].

In this context, the research reported in this investigation presents an approach to design a specimen from which four independent stress states could be simultaneously activated at different regions and for the same load increment to allow measurements that provide the unknown coefficients of a J_3-plasticity type constitutive model developed by Lou et al. This manuscript is organized as follows: section 2 presents details on the J_3-plasticity model and the material information for the representative materials that the reported approach was applied. Section 3 provides details on the design of the complex shaped specimen. Section 4 shows validation efforts which included experiments in which DIC measurements and FEA results were used. The manuscript ends with concluding remarks on the overall usefulness of this approach and possible future steps.

Background

Plasticity model and Finite Element Analysis approach

In this research, we are using the model developed by Lou et al. [10] and which intends to capture both anisotropy and multiple stress-state dependence in the plastic behavior. The Lou model is a J_3 stress invariant type plasticity formulation, capable of describing the complex stress effects that could be present e.g., in metal forming. Equation 1 shows the definition of the yield surface for this model

$$f\left(\sigma_y\right)=a\left(\bar{\varepsilon}_p\right)\left\{b\left(\bar{\varepsilon}_p\right)I_1+\left[\left(J_2^3-c\left(\bar{\varepsilon}_p\right)J_3^2\right)^{1/2}-d\left(\bar{\varepsilon}_p\right)J_3\right]^{1/3}\right\}-\bar{\sigma}_{UT}\left(\bar{\varepsilon}_p\right)=0, \tag{1}$$

where I_1 is a stress invariant of the Cauchy stress tensor, and J_2 and J_3 are the stress invariants of the deviatoric stress tensor. The parameters "a", "b", "c" and "d" that appear in Eq. (1) are determined using experimental data and the four equations summarized in Eq. (2)

$$\left\{\begin{array}{c} a=\frac{\sqrt{3}\bar{\sigma}_{UT}}{\bar{\sigma}_{SS}} \\ b=\frac{1}{3}\left(\frac{\bar{\sigma}_{SS}}{\bar{\sigma}_{PST}}-1\right) \\ d=\frac{24}{7}\left[\left(\frac{\bar{\sigma}_{UT}}{a\bar{\sigma}_{UC}}+b\right)^3-\left(\frac{1}{a}-b\right)^3\right] \\ c=\frac{1}{4}\left\{27-\left[27\left(\frac{1}{a}-b\right)^3+2d\right]^2\right\} \end{array}\right. \tag{2}$$

where $\bar{\sigma}_{\mathrm{UT}}, \bar{\sigma}_{\mathrm{SS}}, \bar{\sigma}_{\mathrm{PST}}$ and $\bar{\sigma}_{\mathrm{UC}}$ are the von Mises equivalent stress at uniaxial tension, shear, plane strain tension and uniaxial compression states, respectively. Parameter "a" in the yield function provides scaling, "b" relates to pressure dependency, "c" defines curvature, and "d" is the strength differential. Based on different values of the hardening parameters and auto-differentiability the yield function can take the shape of yield surfaces such as von-Mises ($a=\sqrt{3}, \mathrm{b}=0, \mathrm{c}=0, \mathrm{~d}=0$), Drucker Prager ($\mathrm{a}, \mathrm{b}, \mathrm{c}, \mathrm{d}=0$), Cazacu Barlat ($\mathrm{a}, \mathrm{b}=0, \mathrm{c}=0, \mathrm{~d}$) etc. Due to this ability of polymorphism, the Lou yield surface is considered as a robust candidate for mechanical behavior characterization. Figure 1 describes the triaxiality vs Lode mapping of the stress states required to calibrate the shape of the yield surface. The corresponding four types of specimen tests, i.e. dogbone (Uniaxial Tension - UT), notched tension (Plane Strain Tension), simple shear and cylinder

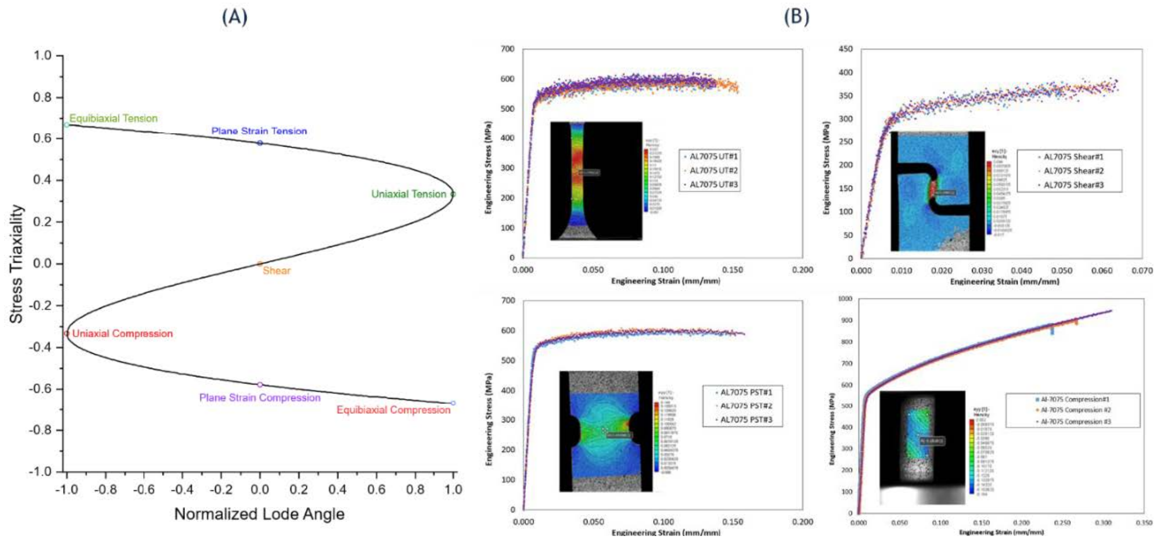

Fig. 1 (A) Lode vs Triaxiality visualization to define several stress states as proposed by Lou et al. [10]; (B) the 4 specimen geometries that correspond to 4 distinct stress states (per Eq. (2)), along with representative stress-strain and full-field metrology data obtained using the Digital Image Correlation (DIC) method

compression (Uniaxial Compression - UC) are required to determine the unknown parameters a, b, c and d , as a function of Equivalent Plastic Strain (EPS).

The implicit associated Lou model was successfully implemented in ABAQUS using a UMAT subroutine with C3D8 type brick elements to perform non-linear analysis of the combination of geometries and their boundary value problems as dictated by standard experimentation setups, procedures, and extracted calibration parameters.

Materials used and experimental setup

Experiments for the evaluation of strain hardening parameters and complex specimen design process were performed using commercial A17075-T6 (procured from OnlineMetals). A servohydraulic frame (MTS 370 Landmark; 100 kN load capacity) was used to impose quasi-static loading conditions with a deformation rate of $0.5\ \mathrm{mm/min}$ applied to five individual stress state geometries including uniaxial tension, plane strain tension, shear, and cylinder and non-conventional compression specimens as shown in Figure 2 [11]. Flat specimen geometries were cut using a waterjet cutter from a 2 mm thick

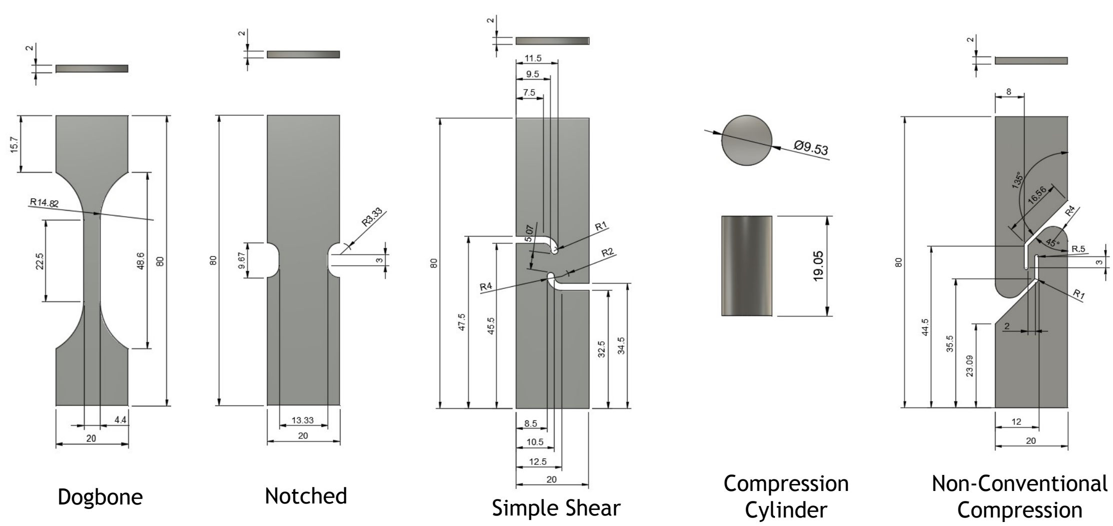

Fig. 2 Test specimen geometries used to obtain the stress-strain behavior of the Al7075-T6 material

sheet. For the compression cylinder specimens, a rod with a 9.525 mm diameter was cut with a 2:1 length-to-diameter ratio.

Full-field displacement and strain measurements were recorded using a stereo DIC system by Correlated Solutions as shown in Figure 3

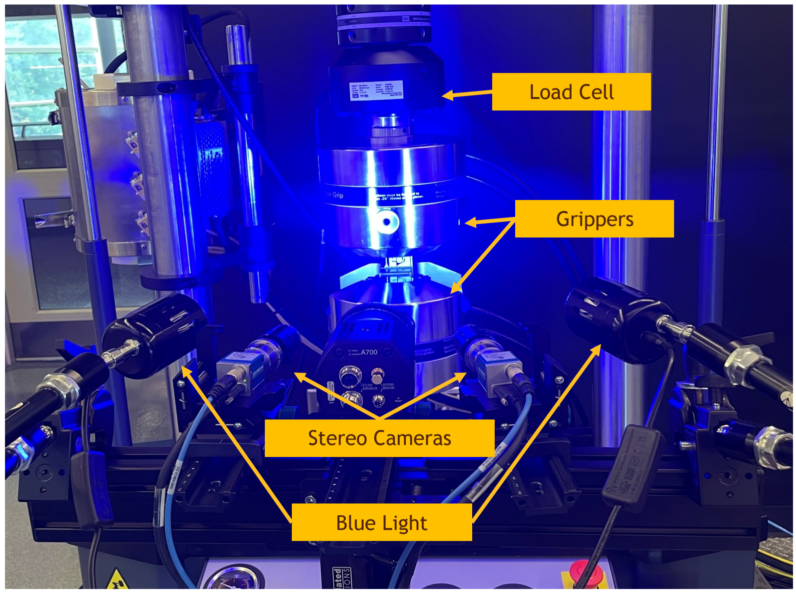

Fig. 3 Mechanical testing setup with DIC stereo system

Details about the testing machine and DIC system are shown in Table 1.

Table 1 Mechanical testing and DIC hardware and software parameters

Fixed Parameters		
	Machine Manufacturer & Model	MTS Landmark
	Grips	Flat wedge grips
	Load Cell	100 kN
	Displacement Rate	$0.5\ \mathrm{mm/min}$
	Data Acquisition Rate	100 Hz
DIC	Image Resolution	2448×2048 pixels
	Lens	Schneider $\mathrm{f}4.0/60\ \mathrm{mm}$
	Image Acquisition Rate	2 Hz
	Patterning Technique	White & Black Spray Paint
	DIC Software	VIC 3D 10, Solution or system?
	Subset Weights	Gaussian
	Interpolant	Optimized 8-tap splines
	Strain Filter Window	15
	Strain Type	Hencky
	Calibration Grid	14×10 dots, 3 mm spacing

The DIC software parameters used are shown in Table 2. These parameters serve as quality control for the mechanical testing of each specimen. Additionally, for each test calibration, projection error, and noise floor measurements were recorded.

Table 2 An example of measured DIC parameters for a tested specimen

Parameters	Average
Noise Floor (με)	19.5
FOV (mm × mm)	54 × 45
In-Plane Measurement Resolution (μm)	0.27
Subset & Step Size (px)	29 × 7
Projection Error (Avg)(< 0.1)	0.032
Calibration Score (< 0.1)	0.029
Magnification (px/mm)	45.58

The a, b, c, d parameters determined for this material and used in this investigation are shown in Figure 4.

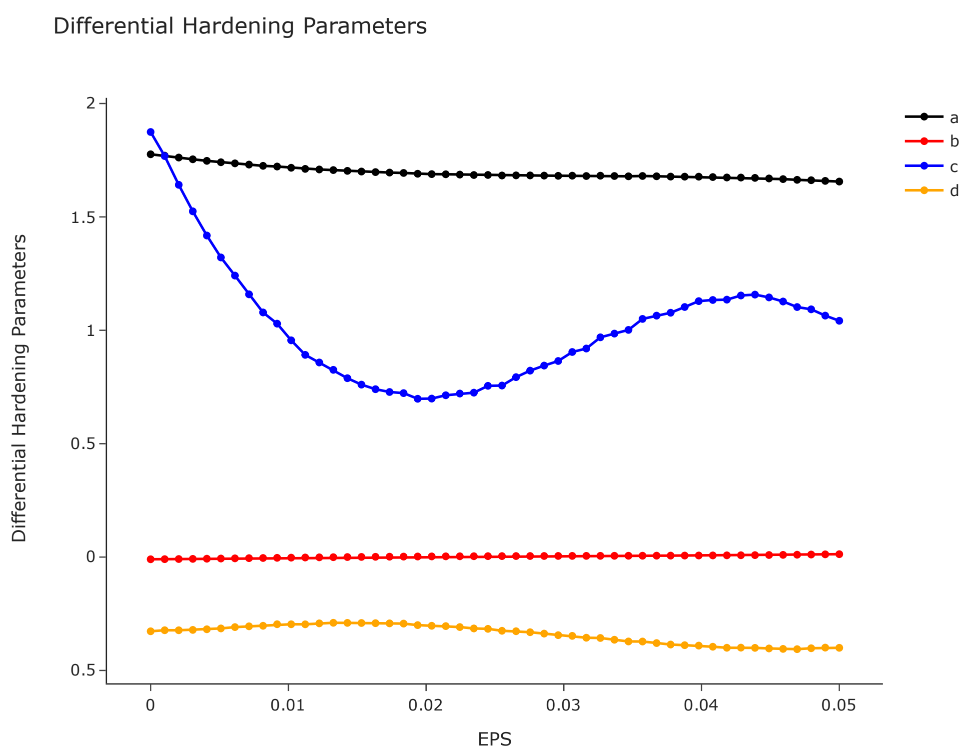

Fig. 4 Differential hardening parameters a, b, c and d for Lou model calibration

Analysis

Complex specimen design

In a multiple stress state specimen, Bensing et al. with the tension/compression and Khameneh et al. with the UT/shear specimen have shown the possibility of simultaneous stress state development on the same specimen [6, 7]. However, deformation associated with one stress state was found to have an adverse effect in localized property extraction such as modulus and poisson ratio, even in the elastic regime. To circumvent this, the following assumption was considered: the material behavior under loading is assumed to be scale independent which allows scaling of the specimen geometry. With this assumption, in elastoplastic materials such as metals, where the linear elastic deformation conforming to Hooke's Law is pronounced, the onset of plasticity at the yield point can be used to calibrate the combined geometry, as explained next.

In the case of combining two specimens such as standard tension and shear specimens, for a given elastoplastic material, experimental results show global loads F_1 and F_2 and overall displacements D_1 and D_2 at yielding, respectively. The geometries of tension and shear specimens can be then non-uniformly scaled such that:

$$F_1 = F_2 \tag{2}$$

$$D_1 = D_2 \tag{3}$$

This ensures simultaneous yielding as well as global load division by a factor (based on the assumed number of regions with independent stress states in the same specimen) to capture stress produced in each scaled specimen geometry.

In the case of a compression specimen, the load vector is in the opposite direction of tension, shear and notch tension specimens. Therefore, the M-specimen was utilized to produce localized compression while the overall geometry is in tension [11]. This special specimen is termed as non-conventional (NC) compression specimen in this work. The NC compression specimen was benchmarked with a standard compression cylinder, as shown in Figure 5 and it was found that the NC compression specimen can recover compression modulus, yield point, and hardening behavior. Since the yield point is used to calibrate the geometry of the combined specimen, the material behavior captured by NC compression specimen was assumed to be adequate for the goals of this investigation. With the reversal of the load vector of compression cylinder, equations Eqs. (3) and (4) extend as follows:

$$F_1 = F_2 = F_3 = F_4 = F_T \tag{4}$$

$$D_1 = D_2 = D_3 = D_4 = D_T \tag{5}$$

The load and displacement equilibration Figure 6–7 does not consider the moments produced by the shear and NCcompression specimen. Due to this, the design of the specimen needs to be such that the moments of these geometries cancel each other out. In the combination geometry, the shear and NC-compression are kept as the central specimens, while the tension and notched tension specimens are at the edges. Also, the NC-compression specimen is placed horizontally flipped as compared to shear specimen. The notches in the notched specimen are scaled uniformly to adhere to ASTM standard to develop plane strain tension stress state. The specimens in the combination geometry are given spaces on either side to allow horizontal deformations and prevent collisions. These steps are crucial to ensure the development of the stress state is similar to the development in individual standard specimens Figure 8.

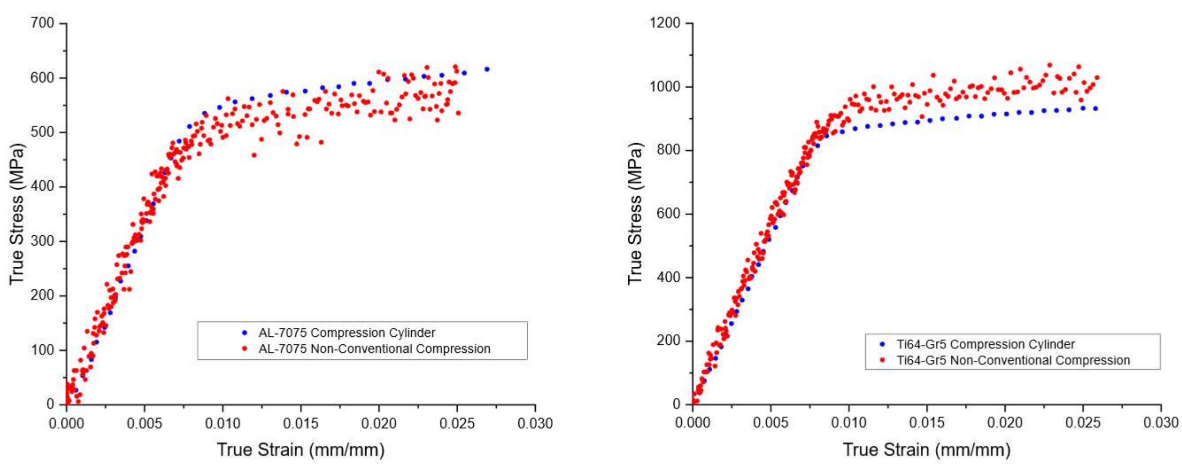

Fig. 5 Comparison of the behavior for the NC compression specimen with respect to ASTM E9 for two commercial materials

The target force parameter $\mathrm{F_T}$ and target displacement parameter $\mathrm{D_T}$ at yielding are calibrated using custom parametric modeling and are conformed to meet the manufacturing constraints of the gauge sections. For the case of A17075-T6, the $\mathrm{F_T}$ and $\mathrm{D_T}$ parameters are calibrated to be 2500 N and 0.45 mm respectively. The specimen is further scaled uniformly to fit a $40\ \mathrm{mm} \times 60\ \mathrm{mm}$ dimension to minimize material usage and maximize number of tests for a given volume of material (Figure 9). This specimen is termed as High Throughput (HTr) in the remainder of this manuscript.

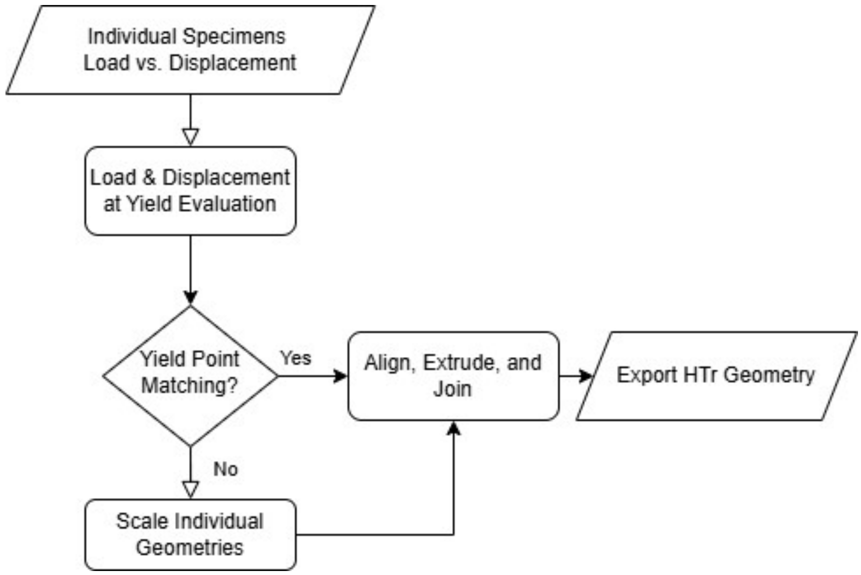

Fig. 6 Overall schematic of the design process for the HTr specimens for each unique material

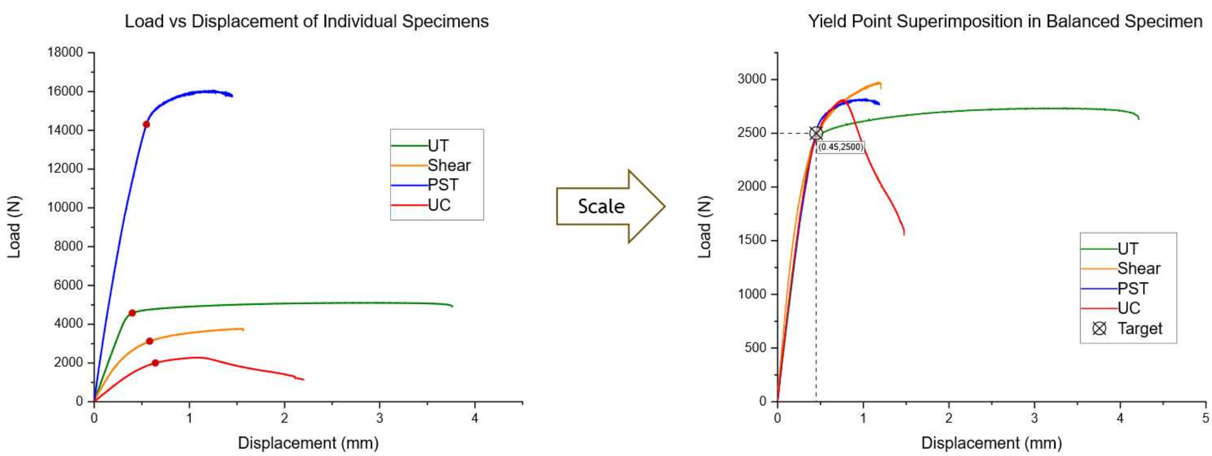

Fig. 7 Scaling of the load-displacement measurements for individual specimens to a common yield load and displacement

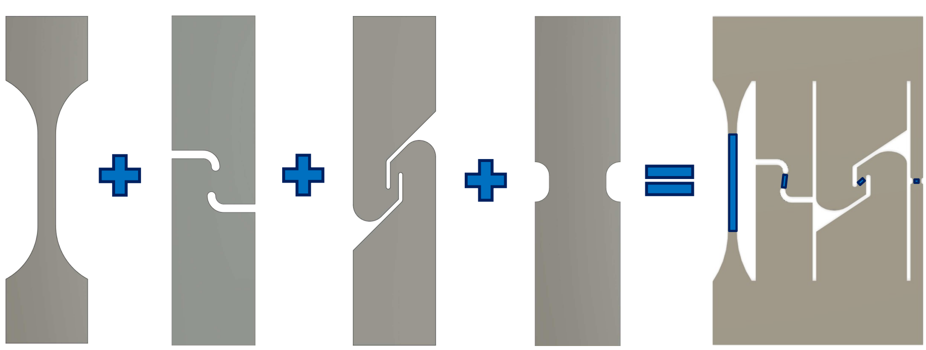

Fig. 8 Combination of the individual specimens to form the complex designed specimen

HTr is simulated with the rigid constraints on the gripping regions and a ramp displacement input at one gripping region while the other is fixed. The J_2 and Lou plasticity models were used in the simulation with the outputs being nodal

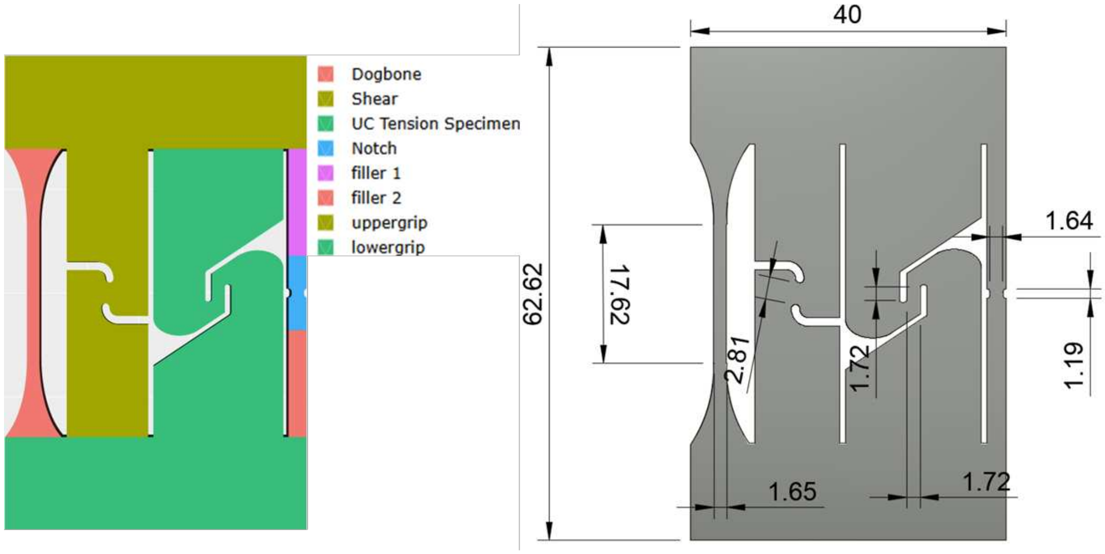

Fig. 9 Left: joining of the individual geometries with gripping and filling areas, right: the generated HTr specimen for a balanced yield load and displacement points for Al7075-T6

displacements, elemental stress and strain for each element as a field output, as well as the global reaction forces. The probing regions were detected using the Lode vs Triaxiality development of the elements in the gauge section of each specimen in HTr (Figure 10). The element groups that showed proper development of Lode and triaxiality for each stress state were combined to form regions of interest to be probed in FEA, as well as experimentation to extract data. From the region of interests in FEA, the average of strains and stresses is extracted as the local stress response for each stress state but also, the load derived stresses were determined using load division by 4 and then further divided by cross section area of each specimen in HTr to capture geometry induced effects. FEA provides the ability to decouple the geometry induced effects and plasticity model defined local response which provides further insight into the performance of the HTr specimen in terms of deviations for expected results.

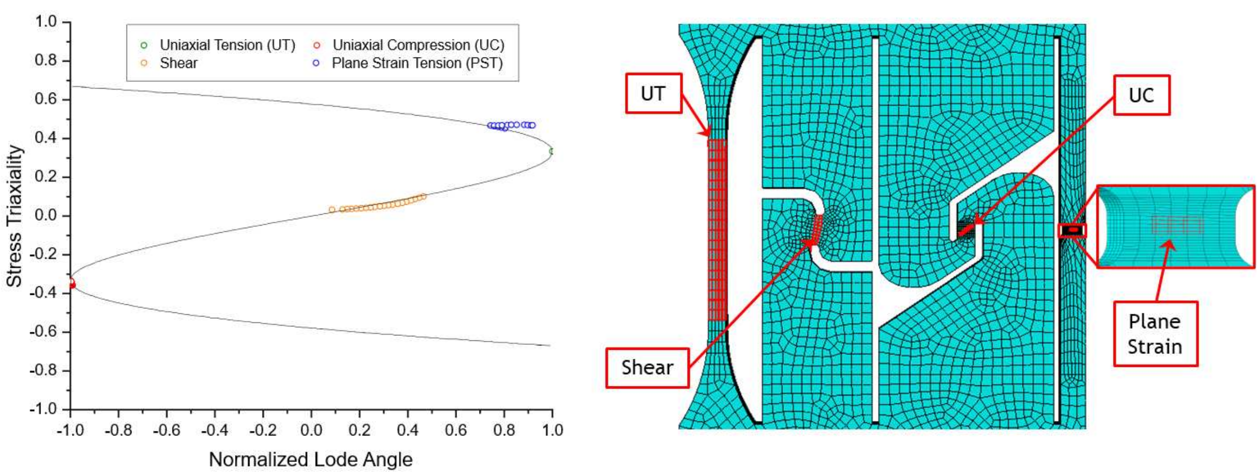

Fig. 10 Validation of the stress mode extracted from the HTr regions of interests (right) with the lode vs. triaxiality plot (right)

Validation

The HTr specimen was loaded experimentally in displacement control until failure. The DIC measurements provided displacement and strain fields as well as global load and displacement measurements. The FEA identified region of interests was utilized to capture the strain of the appropriate stress state. Then, the procedure of derived stresses was followed by utilizing global loads and dividing by 4 to capture the theoretical load experienced by each specimen in HTr specimen. To validate that the HTr specimen can be used to collect DIC data that meet the requirements of the selected J_2 and J_3 plasticity models several computational and experimental steps were taken and shown in the following figures. First, a direct comparison between the full-field strain measurements using DIC and the implemented subroutine of the FEA Lou et al. approach are shown in Figure 11. This shows that the developed FEA subroutine for the HTr specimen is capable of computing correctly all the regions of interest that correspond to the locations where mechanical data needs to be extracted per the J_3 model requirements.

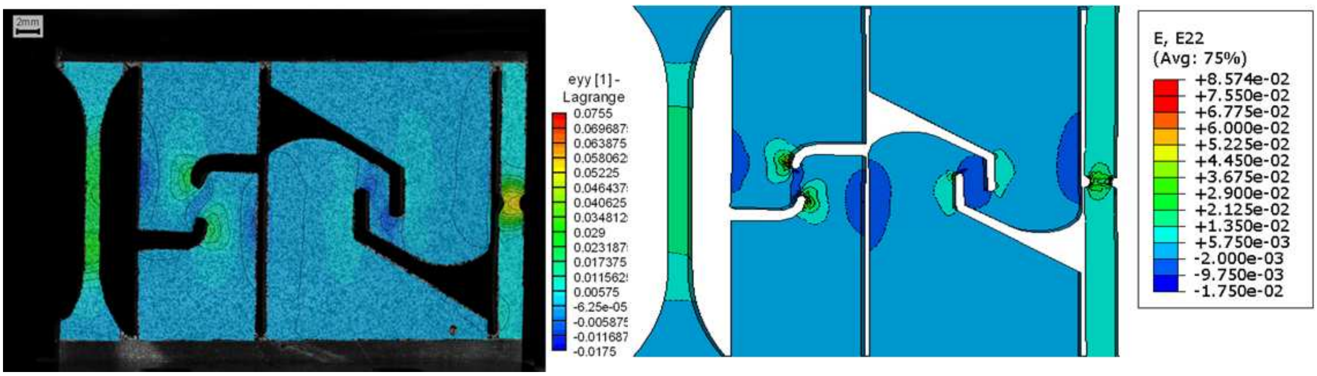

Fig. 11 Full-field strain DIC (left) and FEA(right) outputs scaled to similar contours

A direct comparison between HTr experiments with FEA results for all stress states is shown in Figure 12. The comparison demonstrates success in being capable of using a single complex to collect all data needed for the J_3 model. Additionally, direct comparison of the HTr collected experimental data with individual single stress mode data is shown in Figure 13. A good correlation between the obtained properties from both testing modes is observed.

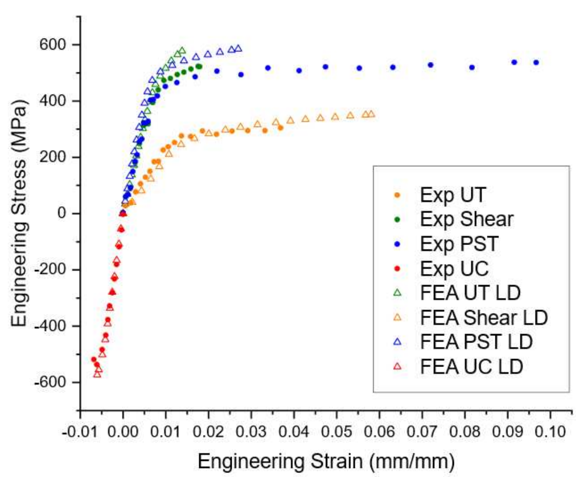

Fig. 12 Comparison of the engineering stress-strain behavior between the HTr experimental behavior to the FEA J_3HTr model

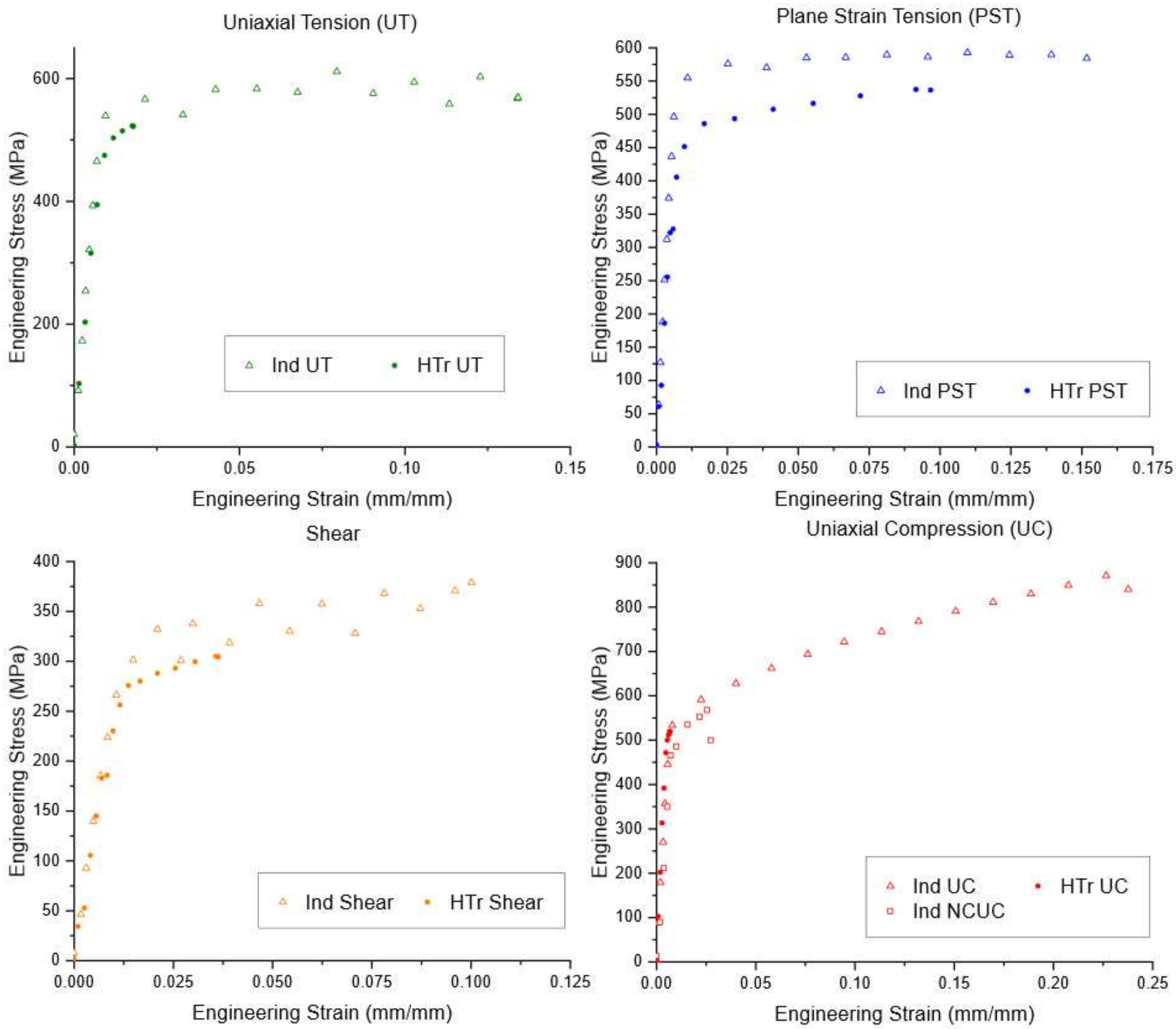

Fig. 13 Comparison of the stress-strain behavior between the individual and HTr specimens

Discussion

Utilizing the inherent advantages of the DIC displacement and strain measurements, the approach in this work showed that data that correspond to multiple stress modes can be extracted simultaneously. The proposed HTr specimen has been validated for commercial A17075-T6 sheet with reliable results. Given four individual stress-strain cures, a unique for composition HTr can be generated and a J_3 plasticity model can then be calibrated. With the data availability of commercial materials, the experimental validation of FEA models can be reduced by a factor of four. If data is not available, at least one test per mode is still required, however, the repeatability of the behavior of the material can still be validated using the HTr specimen.

Concluding Remarks

In this study, an approach of designing a novel specimen was presented that could be used in tandem with a digital image correlation setup to obtain data corresponding to four stress modes needed to calibrate a J_3 plasticity model. Data from four individual specimens tested using conventional geometries, was used to generate this novel specimen and validation results were obtained to support this approach.

Acknowledgments The authors acknowledge the funding from the DARPA Multi-objective Engineering and Testing of Alloy Structures (METALS) research grant number HR001123S0029.

References

1. E. Tekerek et al., "On the process of designing material qualification type specimens manufactured using laser powder bed fusion," *Materials & Design,* vol. 229, p. 111893, 2023.
2. T. Kurzynowski, K. Gruber, W. Stopyra, B. Kuźnicka, and E. Chlebus, "Correlation between process parameters, microstructure and properties of 316 L stainless steel processed by selective laser melting," *Materials Science and Engineering: A,* vol. 718, pp. 64-73, 2018.
3. M. Rossi et al., "Testing methodologies for the calibration of advanced plasticity models for sheet metals: A review," *Strain,* vol. 58, no. 6, p. e12426, 2022.
4. B. Erice, C. C. Roth, and D. Mohr, "Stress-state and strain-rate dependent ductile fracture of dual and complex phase steel," *Mechanics of Materials,* vol. 116, pp. 11-32, 2018.
5. M. A. Sutton, J. J. Orteu, and H. Schreier, *Image correlation for shape, motion and deformation measurements: basic concepts, theory and applications.* Springer Science & Business Media, 2009.
6. T. Bensing and M. Moneke, "Development of a novel testing concept for combined characterisation of tensile and compressive properties," *International Journal of Mechanics and Materials in Design,* vol. 20, no. 5, pp. 895-907, 2024.
7. F. Khameneh, A. Abedini, and C. Butcher, "Experimental and Numerical Fracture Characterization of DP1180 Steel in Combined Simple Shear and Uniaxial Tension," *Metals,* vol. 13, no. 7, p. 1305, 2023.
8. F. Pierron and M. Grédiac, "Towards Material Testing 2.0. A review of test design for identification of constitutive parameters from full-field measurements," *Strain,* vol. 57, no. 1, p. e12370, 2021.
9. E. Jones et al., "Digital image correlation and infrared thermography data for seven unique geometries of 304L stainless steel," *Scientific Data,* vol. 11, no. 1, p. 1101, 2024.
10. Y. Lou, C. Zhang, S. Zhang, and J. W. Yoon, "A general yield function with differential and anisotropic hardening for strength modelling under various stress states with non-associated flow rule," *International Journal of Plasticity,* vol. 158, p. 103414, 2022.
11. D. Mohr and G. Gary, "M-shaped specimen for the high-strain rate tensile testing using a split Hopkinson pressure bar apparatus," *Experimental Mechanics,* vol. 47, pp. 681-692, 2007.